Communications on Applied Nonlinear Analysis
ISSN: 1074-133X
Vol 32 No. 4s (2025)

# Soret and Angle of Inclination Effects on MHD Fluid Flow Past an Upright Porous Plate

**P. Naguru Meeraiah[a], B. Reddappa[b], A. Saila Kumari[c]**

[a]Dept of Mathematics, Research Scholar, JNTUA, Anantapur, A.P., India.

[b]Dept of Mathematics, School of Advanced Sciences, Kalasalingam Academy of Research and Education (Deemed to be University), Krishanankoli, srivilliputhur, Tamil Nadu-626126.

[c]Department of Mathematics, JNTUA College of Engineering, Anantapur, A.P., India.

***Article History:***

***Received:*** *15-09-2024*

***Revised:*** *20-11-2024*

***Accepted:*** *28-11-2024*

**Abstract:**

A theoretical investigation of MHD fluid flow is carried out under the influence of thermal diffusion, chemical reaction, and various factors. The angle of inclination is also taken into account and quantitatively analyzed in this heat and mass transport analysis. The necessary governing equations are numerically resolved using the implicit finite-difference methodology of the Crank-Nicolson type. Graphs depict non-dimensional velocity, fluid temperature and concentration distributions for many fluid parameters involved, such as the joule-heating parameter, suction parameter, chemical reaction parameter, and radiation parameter. The coefficient of skin friction, Nusselt number, and Sherwood number were calculated. The concentration of the fluid increases as the Soret number increases, whereas the Sherwood number decreases.

**Keywords**: Magnetohydrodynamic, Heat and mass transfer, Soret effect, Angle of inclination, Implicit finite difference scheme.

## Introduction

Researchers are very interested in the studies on MHD flows under various geometries because of its importance in Engineering and chemical industries. Zhang et al. [1] evaluated nanofluids' magnetohydrodynamic flow and radiation heat transfer in porous media with variable surface heat flux and chemical reaction. MHD variable viscosity reacting flow over a convectively warmed plate in a porous media with thermophoresis and radiative heat transfer was explained by Makinde et al. [2]. Heat generation/absorption on MHD stagnation flow of nanofluid towards a porous extended sheet with prescribed surface heat flux has been defined by Jalilpour et al. [3]. Raju, Raju et al. [4] examined double solutions for the flow of a nanofluid over a nonlinearly permeable extended sheet in three dimensions. Eddy, the development in film flow down a vertical plate has been clarified by Portalski [5]. Buoyancy-induced flow of non-Newtonian fluids over a non-isothermal horizontal plate embedded in a porous media, Mehta [6]. Takhar et al. [7] analyses the unsteady free convection flow across an infinite vertical porous plate as a result of the combined effects of heat and mass diffusion and a magnetic field. Makinde [8] explained free convection flow with thermal radiation and mass transfer past a moving vertical porous plate with thermal radiation and mass transfer. Chamkha et al. [9] introduced the effect of heat generation or absorption on the thermophoretic free convection boundary layer generated from a vertical flat plate embedded in a porous medium. Mahmoud [10] explained heating the radiation effect on unsteady MHD free convection flow past a vertical plate with temperature-dependent viscosity. Siddiqa et al. [11] identified radiation effects on natural convection

flow over an inclined flat plate with temperature-dependent viscosity. Raju et al. [12] explained the Impacts of an aligned magnetic field and radiation on the flow of ferrofluids over a flat plate with a non-uniform heat source/sink. Khan et al. [13] investigated the flow and heat transfer of ferrofluids over a flat plate with uniform heat flux. Benazir et al. [14] explained the unsteady magnetohydrodynamic Casson fluid flow over a vertical cone and flat plate with a non-uniform heat source/sink.

The current examination is to extend the work of Uwanta and Sani [15] by adding the Soret effect so that systems of equations are coupled. The angle of inclination is also taken as a novelty in this analysis with heat and mass transfer and analyzed numerically. The second-order partial differential equations with boundary conditions are resolved by an implicit finite-difference scheme. The impact of different parameters on non-dimensional parameters, which are velocity, temperature, and fluid concentration of flow, was conferred through figures. The skin friction coefficient and numbers of Nusselt and Sherwood were observed through tables.

**OBJECTIVES**: An incompressible, unsteady, electrically conducting, radiating, heat-absorbing, two-dimensional fluid flow is considered past an infinite porous vertical plate. Let the - axis be taken along the vertical plate towards the upward direction, and the $\bar{y}$ - axis is normal to it. The magnetic fluid $B_0$ is presumed to be acting in the perpendicular direction of the fluid flow. The presence of Soret effect is also considered. Since the length of the plate is infinite, the basic fluid parameters depend on the time $\bar{t}$ and space coordinates $\bar{y}$ only. At the time $\bar{t} \le 0$, both fluid and plate are maintained at the same temperature $\bar{T}_\infty$ and concentration at all points respectively. For a time $\bar{t} > 0$, the plate moves imprudently in its plane with a velocity $\bar{u}$, also the fluid temperature and concentration at the plate are upraised to $\bar{T}_w$ and $\bar{C}_w$ respectively. Based on the above suppositions and the Boussinesq's approximation, the resultant fluid flow equations, i.e., continuity, momentum, mass-energy, and concentration (Sharma et al. 2005, Ahmed et al. 2013), respectively are given below:

$$\frac{\partial \bar{v}}{\partial \bar{y}} = 0 \tag{1}$$

$$\frac{\partial \bar{u}}{\partial \bar{t}} + \bar{v}\frac{\partial \bar{u}}{\partial \bar{y}} = \nu \frac{\partial^2 \bar{u}}{\partial \bar{y}^2} - \frac{\sigma B_0^2 \bar{u}}{\rho} - \frac{\nu \bar{u}}{\bar{K}} + g\bar{\beta} Cos\phi\left(\bar{C} - \bar{C}_\infty\right) + g\beta Cos\phi\left(\bar{T} - \bar{T}_\infty\right) - \bar{b}_1 \bar{u}^2 \tag{2}$$

$$\frac{\partial \bar{T}}{\partial \bar{t}} + \bar{v}\frac{\partial \bar{T}}{\partial \bar{y}} = \frac{1}{\rho C_p}\frac{\partial}{\partial \bar{y}}\left(K\left(\bar{T}\right)\frac{\partial \bar{T}}{\partial \bar{y}}\right) - \frac{1}{\rho C_p}\frac{\partial q_r}{\partial \bar{y}} + \frac{\nu}{C_p}\left(\frac{\partial \bar{u}}{\partial \bar{y}}\right)^2 + \bar{b}\bar{u}^2 - \frac{Q}{\rho C_p}\left(\bar{T} - \bar{T}_\infty\right) \tag{3}$$

$$\frac{\partial \bar{C}}{\partial \bar{t}} + \bar{v}\frac{\partial \bar{C}}{\partial \bar{y}} = D_M \frac{\partial^2 \bar{C}}{\partial \bar{y}^2} + D_T \frac{\partial^2 \bar{T}}{\partial \bar{y}^2} - \bar{R}\left(\bar{C} - \bar{C}_\infty\right)^n \tag{4}$$

The following initial & boundary conditions are

$$\begin{aligned} &\bar{t} \le 0,\ \bar{u}\left(\bar{y},\bar{t}\right) = 0, \bar{T}\left(\bar{y},\bar{t}\right) = \bar{T}_\infty, \bar{C}\left(\bar{y},\bar{t}\right) = \bar{C}_\infty \ \text{for all } \bar{y} < 0 \\ &\bar{t} > 0,\ \bar{u}\left(\bar{y},\bar{t}\right) = 0, \bar{T}\left(\bar{y},\bar{t}\right) = \bar{T}_w, \bar{C}\left(\bar{y},\bar{t}\right) = \bar{C}_w \ \text{ at } \bar{y} = 0 \\ &\qquad \bar{u}\left(\bar{y},\bar{t}\right) = 0, \bar{T}\left(\bar{y},\bar{t}\right) = \bar{T}_\infty, \bar{C}\left(\bar{y},\bar{t}\right) = \bar{C}_\infty \ \text{as } \bar{y} \to \infty \end{aligned} \tag{5}$$

Where $\bar{t}, Q, \bar{T}, \bar{C}, \bar{T}_\infty, \bar{C}_\infty, \bar{T}_w, \bar{C}_w, \nu, B_0, \sigma, \bar{K}, \beta, \bar{b}_1, \bar{\beta}, g, D_T, D_M, \bar{R}, C_P, q_r, \bar{b}, K\left(\bar{T}\right), \rho$ represent dimensional time, volumetric rate of heat generation, temperature of the fluid, species concentration, free stream temperature, free stream concentration, Surface Temperature, surface concentration, kinematic

viscosity, constant magnetic field intensity, Stefan Boltzmann constant, thermal expansion coefficient, Forchheimer parameter of the medium, concentration expansion coefficient, gravitational constant, thermal diffusivity coefficient, chemical molecular diffusivity coefficient, chemical reaction, specific heat at constant pressure, radiative heat flux, joule-heating parameter, the variable thermal conductivity, density. $(\bar{u},\bar{v})$ represents fluid velocity corresponding $\bar{x}$ and $\bar{y}$ directions. The flow geometry is shown in Figure 1. The continuity Eq. (1) on integration, we get $\bar{v}=-v_0,$ for any $v_0>0,$ where $v_0$ is suction velocity. The radiative heat flux can be written by Rosseland approximation as

$$\frac{\partial q_r}{\partial \bar{y}}=-4\sigma\bar{a}\left(\bar{T}_\infty^4-\bar{T}^4\right) \tag{7}$$

Now we expanding $\bar{T}^4$ into about $\bar{T}_\infty$ in series form, we get

$$\bar{T}^4 \approx 4\left(\bar{T}-\bar{T}_\infty\right)\bar{T}_\infty^3+\bar{T}_\infty^4 \approx 4\bar{T}\bar{T}_\infty^3-3\bar{T}_\infty^4 \tag{8}$$

The temperature-dependent variable thermal conductivity (Abel et al. 2009) is given by

$$K\left(\bar{T}\right)=\left[\delta(\bar{T}-\bar{T}_\infty)+1\right]k_\alpha \tag{9}$$

where the $k_\alpha$ is the fluid thermal conductivity and $\delta$ is the constant.

**Methods**: The following non-dimensional variables are defined to obtain non-dimensional partial differential equations (PDE)

$$\begin{aligned}
&U=\frac{\bar{u}}{U_0},y=\frac{\bar{y}U_0}{\nu},t=\frac{\bar{t}U_0^2}{\nu},\theta=\frac{\bar{T}-\bar{T}_\infty}{\bar{T}_w-\bar{T}_\infty},C=\frac{\bar{C}-\bar{C}_\infty}{\bar{C}_w-\bar{C}_\infty},\tau=\delta\left(\bar{T}-\bar{T}_\infty\right),b=\frac{\bar{b}\nu}{\bar{T}_w-\bar{T}_\infty},\\
&Sc=\frac{\nu}{D_M},\Pr=\frac{\nu\rho C_P}{k_\alpha},Ec=\frac{U_0^2}{C_P\left(\bar{T}_w-\bar{T}_\infty\right)},Gr=\frac{g\beta\nu\left(\bar{T}_w-\bar{T}_\infty\right)}{U_0^3},Gc=\frac{g\bar{\beta}\nu\left(\bar{C}_w-\bar{C}_\infty\right)}{U_0^3},\\
&\alpha=\frac{v_0}{U_0},K=\frac{\bar{K}U_0^2}{\nu},N=\frac{16\bar{a}\sigma\bar{T}_\infty^3\nu^2}{k_\alpha U_0^2},M=\frac{\nu\sigma B_0^2}{\rho U_0^2},b_1=\frac{\bar{b}_1\nu}{U_0},S=\frac{Q\nu^2}{k_\alpha U_0^2},\\
&S_0=\frac{D_T}{\nu}\left(\frac{\bar{T}_w-\bar{T}_\infty}{\bar{C}_w-\bar{C}_\infty}\right),Kr=\frac{\nu\bar{R}\left(\bar{C}_w-\bar{C}_\infty\right)^{n-1}}{U_0^2}
\end{aligned} \tag{10}$$

Where $U_0$ is the non-dimensional constant.

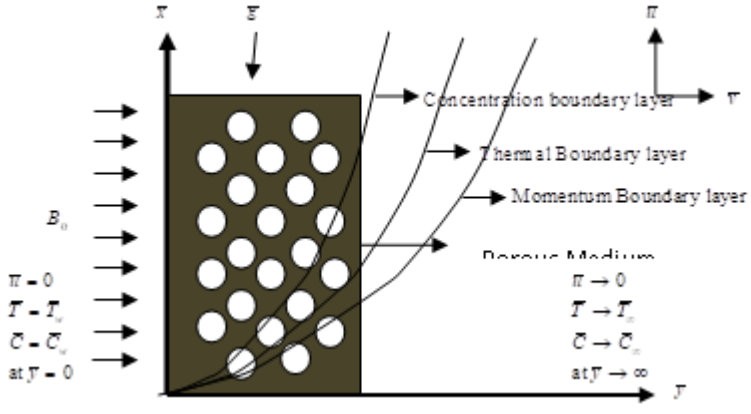


Fig. 1. Flow geometry and coordinate system

By introducing the above dimensionless variables from equation (10), then the Equations (2)-(4) converted as follows:

$$\frac{\partial U}{\partial t}-\alpha\frac{\partial U}{\partial y}=\frac{\partial^2 U}{\partial y^2}-\left(M+\frac{1}{K}\right)U+GrCos\phi\theta+GcCos\phi C-b_1U^2 \tag{11}$$

$$\frac{\partial\theta}{\partial t}-\alpha\frac{\partial\theta}{\partial y}=\frac{(1+\tau\theta)}{\Pr}\frac{\partial^2\theta}{\partial y^2}+\frac{\tau}{\Pr}\left(\frac{\partial\theta}{\partial y}\right)^2+\frac{(S-N)}{\Pr}\theta+Ec\left(\frac{\partial U}{\partial y}\right)^2+bU^2 \quad (12)$$

$$\frac{\partial C}{\partial t}-\alpha\frac{\partial C}{\partial y}=\frac{1}{Sc}\frac{\partial^2 C}{\partial y^2}+S_0\frac{\partial^2\theta}{\partial y^2}-KrC \quad (13)$$

From Eq. (5), Initial & boundary conditions are

$$\left.\begin{aligned} t\le 0 \ \&\ \text{y<0}:\ U(y,t)=0,\ \theta(y,t)=0, C(y,t)=0\\ t>0 \ \&\ \text{y=0}:\ U(y,t)=0,\ \theta(y,t)=1, C(y,t)=1\\ U(\infty,t)=0,\ \theta(\infty,t)=0, C(\infty,t)=0 \end{aligned}\right\} \quad (14)$$

Where $U,\Pr,b_1,\theta,C,Sc,Ec,Gc,M,K,N,\alpha,\tau,Kr,b,Gr,S,So$ represents dimensionless velocity, Prandtl number, inertia number, dimensionless temperature, dimensionless species concentration, Schmidt number, Eckert number, mass Grashof number, magnetic field, porosity, radiation, suction, variable thermal conductivity, chemical reaction, dimensionless joule-heating parameter, thermal Grashof number, heat source parameters, Soret number.

Equations (11)-(13) are 2nd order non-linear coupled PDE together with both conditions from the equation (14). So these equations (11)-(14) are resolved by using the Crank-Nicolson implicit finite-difference scheme. Therefore, finite-difference equations are mention below:

$$-r_1U_{i-1}^{j+1}+(1+2r_1)U_i^{j+1}-r_1U_{i+1}^{j+1}=r_2U_{i-1}^{j}+(-r_4-\alpha r_3-2r_2+1)U_i^{j}+ (\alpha r_3+r_2)U_{i+1}^{j}+\Delta tGrCos\phi\theta_i^{j}+GcCos\phi\Delta tC_i^{j}-b_1\Delta t\left(U_i^{j}\right)^2 \quad (15)$$

$$-qr_1\theta_{i-1}^{j+1}+(\Pr+2qr_1)\theta_i^{j+1}-qr_1\theta_{i+1}^{j+1}=qr_2\theta_{i-1}^{j}+(\Pr-2qr_2-\alpha\Pr r_3-N\Delta t+S\Delta t)\theta_i^{j}+ (qr_2+\alpha\Pr r_3)\theta_{i+1}^{j}+\tau r_5\left(\theta_{i+1}^{j}-\theta_{i-1}^{j}\right)^2+\Pr Ecr_5\left(U_{i+1}^{j}-U_{i-1}^{j}\right)^2+\Pr\Delta tb\left(U_i^{j}\right)^2 \quad (16)$$

$$-r_1C_{i-1}^{j+1}+(Sc+2r_1)C_i^{j+1}-r_1C_{i+1}^{j+1}=r_2C_{i-1}^{j}+(Sc-2r_2-\alpha Scr_3-KrSc\Delta t)C_i^{j}+ (r_2-\alpha r_3Sc)C_{i+1}^{j}+2ScS_0r_1\theta_{i-1}^{j}-4ScS_0r_1\theta_i^{j}+2ScS_0r_1\theta_{i+1}^{j} \quad (17)$$

$$\text{where } r_1=r_2=\frac{\Delta t}{2(\Delta y)^2}, r_3=\frac{\Delta t}{\Delta y}, r_4=\Delta t\left(M+\frac{1}{K}\right), r_5=\frac{\Delta t}{4(\Delta y)^2}, q=1+\tau\theta_i^{j} \quad (18)$$

Here $(i,j)$ is an arbitrary grid point in the discrete mesh system. Where indices $i\&j$ refer to $y\&t$ respectively. The discrete mess system can be divided by rectangles whose length $\Delta y=0.1$ and width $\Delta t=0.001$. Also, consider $i_{\max}=200$ and $j_{\max}=500$. Then the equation (14) can be expressed in terms of finite-difference form for any $i,j$

$$\left.\begin{aligned} U(i,0)=0,\ U(0,j)=0,\ U(i_{max},j)=0\\ \theta(i,0)=0,\ \theta(0,j)=1,\ \theta(i_{max},j)=0\\ C(i,0)=0,\ C(0,j)=1,\ C(i_{max},j)=0 \end{aligned}\right\} \quad (19)$$

From the equations (15)-(17) with the above initial and boundary conditions, every internal node of each time step constitutes a tridiagonal matrix. The dimension of tridiagonal matrix is $i_{\max}-1\times i_{\max}-1$. The tridiagonal matrix system of equations can be resolved by using the Thomas algorithm for solving $i_{\max}-1$ equations with $i_{\max}-1$ unknowns for each time step. Since it is a coupled equation, we started to compute the concentration and temperature distributions at each time step from equation (17) and

equation (16), respectively, and then calculated values are used to compute the velocity distribution at each time step from equation (15) which meets the convergence criteria. The non-dimensional parameters, which are the skin friction coefficient, Nusselt and Sherwood numbers, can be calculated by the following formulas, respectively.

$$Cf = \frac{\partial U}{\partial y}, Nu = -\frac{\partial \theta}{\partial y}, Sh = -\frac{\partial C}{\partial y} \text{ at y=0}$$

**Results**:

Mathematical equations are formulated and solved numerically for the problem on Soret and variable thermal conductivity effects on heat and mass transfer flow past an infinite and inclined vertical plate. The values of parameters are fixed throughout the simulations except if, in any case, expressed. That is $Gr$ =1.00, $\tau$ =0.10, $Sc$ = 0.62, $Kr$ =0.10, $Ec$ =0.01, Pr = 0.71, $b$ =1.00, $M$ =1.00, $So$ =1.00, $K$ =1.00, $Gc$ =1.00, $N$ =0.10, $b_1$ =1.00, $S$ =1.00, $\alpha$ = 1.00,

$n$ =1.00.

Velocity distributions are presented from Fig. 2 to Fig. 10 for diverse values of $M, K, Gr, Gc, N, \alpha, \tau, Kr, So.$ Fig. 2 exhibits $U$ for different values of $M$ =1, 5, 10, and 15. This figure indicates $U$ falls with an increment in the values of $M$ . This is because of an increment that $M$ shows the effect on free convective flow. The variation in $U$ with $K$ is presented in Fig. 3. A higher permeable parameter improves the fluid velocity. Naturally, the resistance of the fluid flow might be ignored due to an increment in the size of the holes of a porous medium. The influence of $\alpha$ on $U$ completely coincides with the effect of the radiation parameter as clearly observed in Fig. 4. Fig. 5 presents the effect of $\tau$ on $U$ . It is identified fluid velocity increases with increasing $\tau$ . Figure 6 shows that the velocity decreases on increasing the angle of inclination. It is observed that $\theta$ decreases whenever $\alpha$ increased. Fig. 7 demonstrates $\theta$ rises with an increment in the values of $\tau$ and in the same way for Fig. 8, $\theta$ increase for the growth in the values of $S$ .

The effect of $Sc$ on $C$ is presented in Fig. 9. The trend shows $C$ reduction with augmented values of $Sc$ due to the increase of $Sc$ means to fall in molecular diffusion. Fig. 10 sketched the effect of $\alpha$ on $C$ . It notices that the non-dimensional concentration falls with an increment of $\alpha$ .

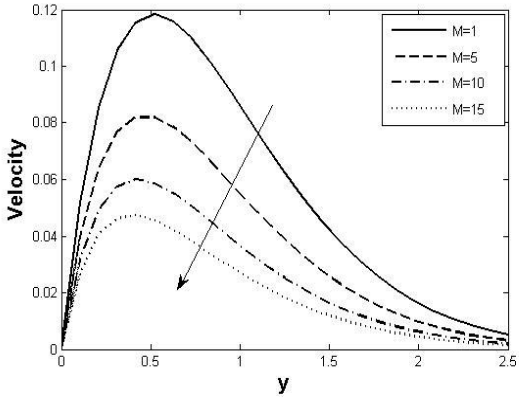


**Fig. 2. Velocity against y for $M$ =1, 5, 10, and 15.**

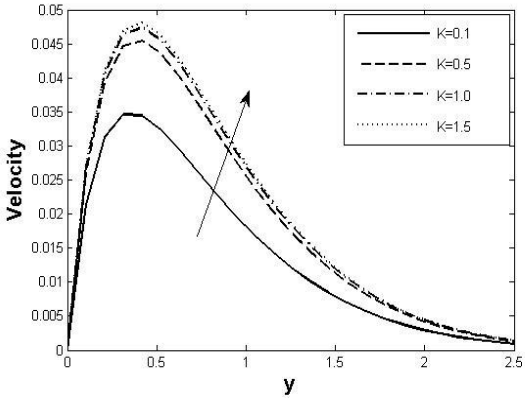


**Fig. 3. Velocity against y for $K$ =0.1, 0.5, 1, and 1.5.**

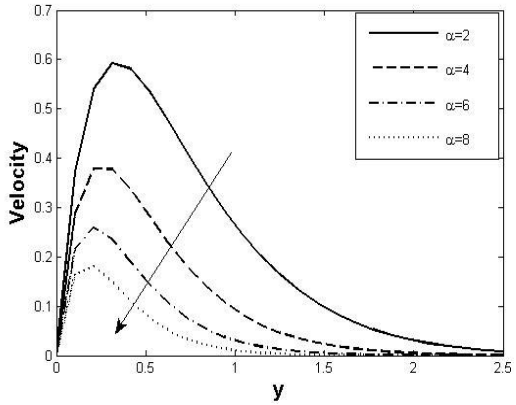


**Fig. 4.** Velocity against y for $\alpha$ =2, 4, 6 and 8.

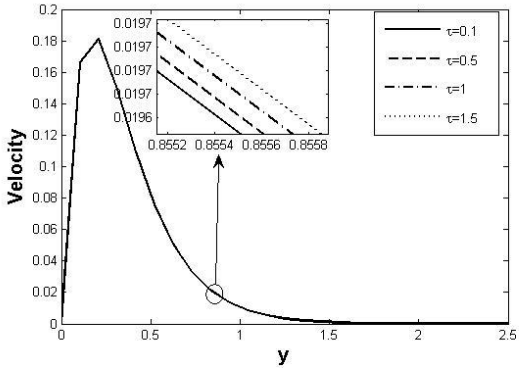


Fig. 5. Velocity against y for $\tau$ =0.1, 0.5, 1, and 1.5.

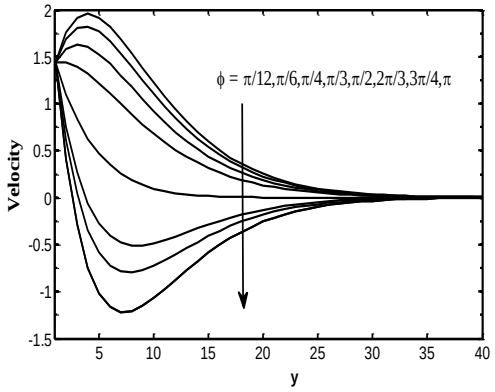


**Fig. 6.** Velocity against y for

$$\phi = \frac{\pi}{12}, \frac{\pi}{6}, \frac{\pi}{4}, \frac{\pi}{3}, \frac{2\pi}{3}, \frac{3\pi}{4}, \pi$$

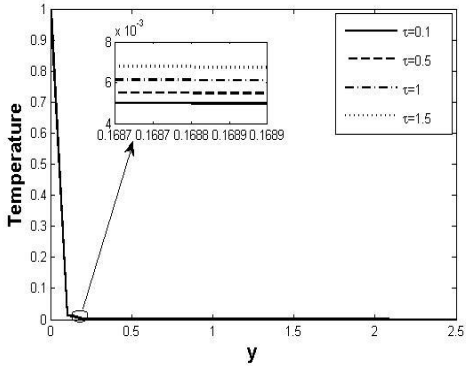


**Fig. 7.** Temperature against y for $\tau$ =0.1, 0.5, 1, and 1.5.

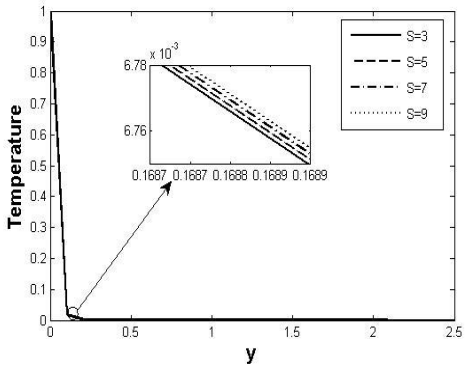


**Fig. 8.** Temperature against y for $S$ =3, 5, 7, and 9.

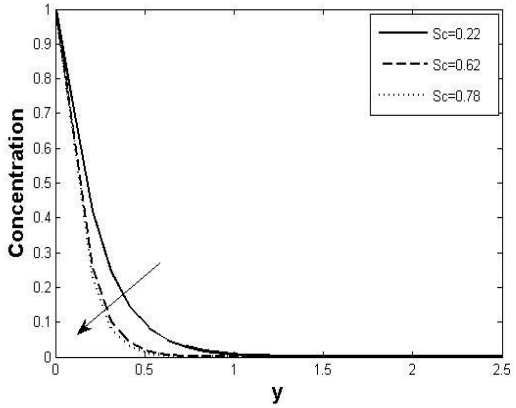


Fig. 9. Concentration against y for $Sc$ =0.22, 0.62, and 0.78

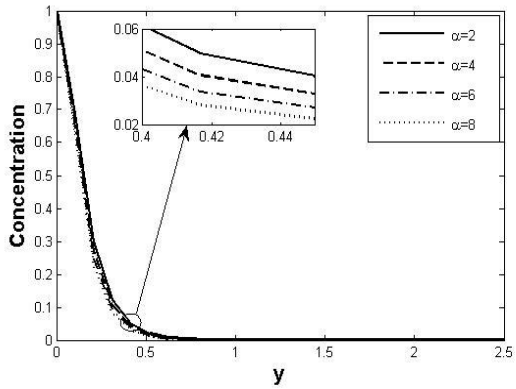


**Fig. 10.** Concentration against y for $\alpha$ =2, 4, 6, and 8.

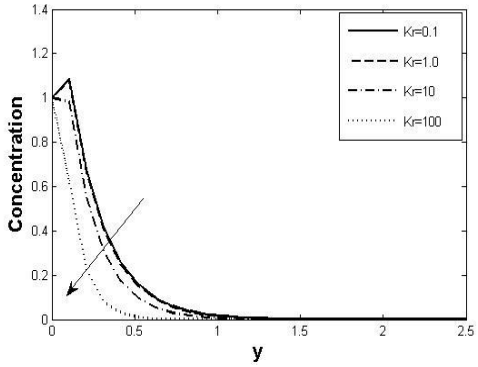


Fig. 11. Concentration against y for $Kr$ =0.1, 1.0, 10, and 100.

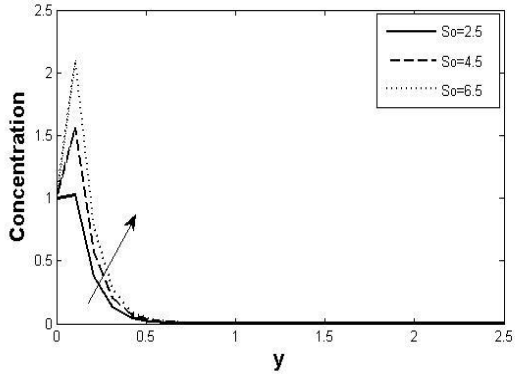


**Fig. 12.** Concentration against y for $So$ = 2.5, 4.5, and 6.5.

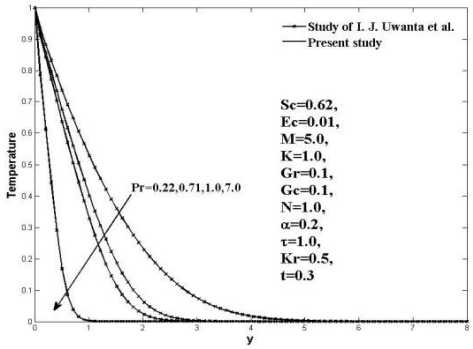


Fig. 13. Comparison of present results with that obtained by Uwanta et al. [14] with $b_1 = 0, So = 0, S = 0, b = 0.$

The influence of $Kr$ on $C$ is shown in Fig. 11. It is noticed from the figure, $C$ is decrease whenever increasing the values of $Kr$. Because of the large values of $Kr$ to decrease the thickness of the solutal boundary layer and raise the mass transfer of the fluid. The influence of $So$ on $C$ opposes the influence of chemical reaction $Kr$ as shown in Fig. 12. Fig. 13 exhibits the validity of the outcomes compared with the fluid temperature for values of $\Pr$. We equate the outcomes with the existing outcomes obtained by Uwanta et al. [14] by removing the inertia number, joule-heating parameter, heat source, and Soret parameters It shows that there is complete concurrence in their results.

Table 1 to table 3 presents the non-dimensional values of coefficient of Skin friction ($Cf$) and numbers of Nusselt ($Nu$) and Sherwood ($Sh$) for the numerical solution of governing equations. Table 1 displays the influence of non-dimensional parameters $\Pr, \alpha, Gr, So, Sc, Kr, M, N, S$ and $Gc$ on $Cf$. In table 1, it is observed that the augmenting values of $Pr, Kr, M, N, Sc$ and $\alpha$ leads to a decline in $Cf$ but for ascending values of $Gr, Gc, S$ and $So$ rises in $Cf$. Table 2 presents the influence of non-dimensional parameters $\Pr, Gr, N, b, \alpha$ and $So$ on $Nu$. From Table 2, observe $Nu$ rises with increasing the values of $\Pr, N$ and $\alpha$ but increasing the values of $Gr, b$ and $So$ results fall of $Nu$. Similarly, table 3 exhibits the influence of non-dimensional parameters $Sc, Kr, \alpha$ and $So$ on $Sh$. Results from table 3 show that $Sh$ increases whenever the values of $Sc, Kr$ and $\alpha$ increases but increasing $So$ leads to a decrease of $Sh$.

| Pr | *Gr* | *Gc* | *Sc* | *Kr* | $\alpha$ | *M* | *N* | *S* | *So* | *Cf* |
|---|---|---|---|---|---|---|---|---|---|---|
| 0.71 | 1 | 1 | 0.62 | 0.1 | 1 | 1 | 0.1 | 1 | 1 | 0.7145 |
| 1 | | | | | | | | | | 0.6811 |
| | 5 | | | | | | | | | 2.0936 |
| | 8 | | | | | | | | | 3.1401 |
| | | 5 | | | | | | | | 2.1216 |
| | | 8 | | | | | | | | 3.1231 |
| | | | 0.78 | | | | | | | 0.6967 |
| | | | 0.90 | | | | | | | 0.6857 |
| | | | | 1 | | | | | | 0.6871 |
| | | | | 2 | | | | | | 0.6617 |
| | | | | | 4 | | | | | 0.5248 |
| | | | | | 6 | | | | | 0.3742 |
| | | | | | | 5 | | | | 0.5340 |
| | | | | | | 10 | | | | 0.4143 |
| | | | | | | | 1 | | | 0.6898 |
| | | | | | | | 5 | | | 0.6305 |
| | | | | | | | | 3 | | 0.8042 |
| | | | | | | | | 5 | | 0.9927 |
| | | | | | | | | | 2.5 | 0.7927 |
| | | | | | | | | | 4.5 | 0.8957 |

**Table 1.** Coefficient of Skin friction

| Pr | *Gr* | *N* | *b* | $\alpha$ | *So* | *Nu* |
|---|---|---|---|---|---|---|
| 0.71 | 1 | 0.1 | 1 | 1 | 1 | 0.5522 |
| 1 | | | | | | 0.8803 |
| | 5 | | | | | 0.4924 |
| | 8 | | | | | 0.4092 |
| | | 1 | | | | 0.9379 |
| | | 5 | | | | 1.9686 |
| | | | 10 | | | 0.4766 |
| | | | 50 | | | 0.1155 |
| | | | | 4 | | 1.8389 |
| | | | | 6 | | 2.6383 |
| | | | | | 2.5 | 0.5484 |
| | | | | | 4.5 | 0.5422 |

**Table 2.** Nusselt number

| *Sc* | *Kr* | $\alpha$ | *So* | *Sh* |
|---|---|---|---|---|
| 0.62 | 0.1 | 1 | 1 | 0.7722 |
| 0.78 | | | | 0.8853 |
| | 1 | | | 1.0320 |

| | | | | |
|---|---|---|---|---|
| | 2 | | | 1.2747 |
| | | 4 | | 1.1867 |
| | | 6 | | 1.5564 |
| | | | 2.5 | 0.4890 |
| | | | 4.5 | 0.1187 |

**Table 3.** Sherwood number

**Conclusions**:

The significant conclusions are made as follows

- Rising of angle of inclination leads to decrease the velocity.
- The influence of $\alpha$ and $So$ on $Nu$ is quite the opposite to that of the temperature $\theta$ of the fluid.
- The influence of $Sc, \alpha, Kr$ and $So$ on $Sh$ is quite the opposite to that of the concentration $C$ of the fluid.

The effect of concentration $C$ of the fluid rises with an increased Soret number $So$ whereas reduces in Sherwood number $Sh$.

**Refrences**

[1] Zhang, C., Zheng, L., Zhang, X., Chen, G., MHD flow and radiation heat transfer of nanofluids in porous media with variable surface heat flux and chemical reaction, Appl. Math. Model., 39, pp. 165–181, 2015.
[2] Makinde, O.D., Khan, W.A., Culham, J.R., MHD variable viscosity reacting flow over a convectively heated plate in a porous medium with thermophoresis and radiative heat transfer, Int. J. Heat Mass Transfer, 93, pp. 595–604, 2016.
[3] Jalilpour, B., Jafarmadar, S., Ganji, D.D., Shotorban, A.B., Taghavifar, H., Heat generation/absorption on MHD stagnation flow of nanofluid towards a porous stretching sheet with prescribed surface heat flux, J. Mol. Liq., 195, 94–204, 2014.
[4] Raju, C.S.K., Sandeep, N., Jayachandra Babu, M., Sugunamma, V., Dual solutions for three-dimensional MHD flow of a nanofluid over a nonlinearly permeable stretching sheet, Alexandria Eng. J., 55 (1), pp. 151–162, 2016.
[5] Portalski, S., Eddy formation in film flow down a vertical plate, Ind. Eng. Chem. Fundam, 3 (1), pp. 49–53, 1964.
[6] Mehta, K.N., Narasimha Rao, K., Buoyancy induced flow of non-Newtonian fluids over a non-isothermal horizontal plate embedded in a porous medium, Int. J. Eng. Sci., 32 (3), pp. 521–525, 1994.
[7] Takhar, H.S., Roy, S., Nath, G., Unsteady free convection flow over an infinite vertical porous plate due to the combined effects of thermal and mass diffusion, magnetic field and Hall currents, Heat Mass Transf., 39, 825–834, 2003.
[8] Makinde, O.D., Free convection flow with thermal radiation and mass transfer past a moving vertical porous plate, Int. Commun. Heat Mass Transf., 32, pp. 1411–1419, 2005.
[9] Chamkha, A.J., Al-Mudhaf, A.F., Pop, I., Effect of heat generation or absorption on thermophoretic free convection boundary layer from a vertical flat plate embedded in a porous medium, Int. Commun. Heat Mass Transf., 33, pp. 1096–1102, 2016.
[10] Mahmoud, M.A.A., Thermal radiation effect on unsteady MHD free convection flow past a vertical plate with temperature dependent viscosity, Can. J. Chem. Eng., 87, pp. 47–52, 2007.
[11] Siddiqa, S., Asghar, S., Hossain, M.A., Radiation effects on natural convection flow over an inclined flat plate with temperature-dependent viscosity, Proc. Inst. Mech. Engineers, Part C: J. Mech. Eng. Sci., 225 (2), pp. 407–419, 2011.
[12] Raju, C.S.K., Sandeep, N., Sulochana, C., Sugunamma, V., Effects of aligned magneticfriеld and radiation on the flow of ferrofluids over a flat plate with non-uniform heat source/sink, Int. J. Sci. Eng., 8 (2), pp. 151–158, 2015.
[13] Khan, W.A., Khan, Z.H., Haq, R.U., Flow and heat transfer of ferrofluids over a flat plate with uniform heat flux, Eur. Phys. J. Plus, 130 (4), pp. 1–10, 2015.
[14] Benazir, A.J., Sivaraj, R., Makinde, O.D., Unsteady magnetohydrodynamic Casson fluid flow over a vertical cone and flat plate with non-uniform heat source/sink, Int. J. Eng. Res. Africa, 21, pp. 69–83, 2016.
[15] Uwanta IJ Sani M (2014). Heat Mass Transfer Flow past an Infinite Vertical Plate with Variable Thermal Conductivity, Heat Source and Chemical Reaction, *Int. J. Eng. Sci.,* 3(5), 77-89.